

## Preparation of Ti/Sb-SnO<sub>2</sub>-GO/PbO<sub>2</sub> Electrode and Its Application in Electrochemical Oxidation Treatment of Ultralow-Concentration Residual Hydrazine in Water

Zhike Tang<sup>1+</sup>, Junjie Zhou<sup>1+</sup>, Li Qi<sup>1</sup>, Lei Liu<sup>1</sup>, Shu`ang Li<sup>1</sup>, Hongbin Sun<sup>1,\*</sup>, Gang Zhang<sup>1,\*</sup>

Department of Chemistry, Northeastern University, Shenyang 110819, P.R. China.

+ These two authors are both the co-first author of the paper.

\*E-mail: [sunhb@mail.neu.edu.cn](mailto:sunhb@mail.neu.edu.cn), [gangzhang99@126.com](mailto:gangzhang99@126.com)

Received: 25 October 2016 / Accepted: 28 February 2017 / Published: 12 April 2017

---

A novel Ti/Sb-SnO<sub>2</sub>-GO/PbO<sub>2</sub> electrode was prepared for the water treatment technology. The Sb-SnO<sub>2</sub>-GO layer was successfully prepared by thermal deposition on Ti substrate, and the PbO<sub>2</sub> film was loaded as the working surface by electrodeposition method. Both of the preparation process of the interlayer Sb-SnO<sub>2</sub>-GO and PbO<sub>2</sub> coatings were optimized. The electrochemical degradation of hydrazine hydrate was investigated in different conditions using the optimized electrode. The results showed that the electrochemical oxidation was so efficient that the ultralow-concentrated hydrazine was almost completely removed from water.

---

**Keywords:** Electrochemical Oxidation; Hydrazine; Electrodeposition; PbO<sub>2</sub> electrode; Kinetics

### 1. INTRODUCTION

With the development of the technologies, the requirement of newer chemicals has been increasing. Some of the chemicals turn into pollutants in water, so a number of researchers have devoted into the development of water treatment to seek the technology that takes advantage of high efficiency and low energy consumption. Electrochemical oxidation is a potential water treatment technology to solve this environmental problem [1-4]. By this way, the pollutants are destroyed by directly or indirectly electrochemical oxidation, and no additional chemical is required, which may cause the secondary pollution [5-7]. Therefore, this technology gains increasing attention because of its mild reaction conditions, relatively low energy consumption, simple operations, and easy to combine with other technologies [8-10].

Hydrazine hydrate is an important chemical, which is widely used in pharmaceutical, dyes, military, aerospace and other fields [11]. But it is worth noting that the hydrazine hydrate seriously injures human's internal organs, blood system and nervous system [12, 13], and its toxicity can be

accumulated. At present, hydrazine hydrate has been recognized as one of the important harmful substances as a carcinogen [14]. According to the national standard of China, the maximum allowable concentration of hydrazine hydrate in surface water is 0.01mg/L. The treatment of hydrazine in wastewater has attracted much attention [15].

The electrochemical degradation is a safe, efficient and convenient water treatment method. DSA (Dimensional Stable Anode) electrode is a type of high efficiency and energy saving electrode that had been developed since 1950s. Titanium is usually used as the substrate, and a metal oxide such as  $\text{IrO}_2$  [16],  $\text{RuO}_2$  [17],  $\text{Pt}$  [18],  $\text{SnO}_2$  [19] or  $\text{PbO}_2$  [20] is coated on the surface. It is an ideal anode material for electrochemical treatment of wastewater for its high oxygen over-potential, stability and relative low cost [21]. But the service life of  $\text{Ti/Sb-SnO}_2\text{-GO}$  electrode is short which limits its further applications [22]. Lead oxide electrode is widely used in electro-synthesis [23, 24], lead-acid battery [25, 26] and organic wastewater treatment [27] because of its high oxidation potential, good electrochemical stability and low cost. However, some defects of  $\text{PbO}_2$  electrode limit its further application in industry [28, 29]. The adhesion of the oxides active layer ( $\text{PbO}_2$ ) and the substrate isn't strong enough and the internal stress is great, so the  $\text{PbO}_2$  coating layer is easy to detach [30]. This may lead to the collapse of active layer. Therefore, various ways have been explored to improve the  $\text{PbO}_2$  electrode, such as modifying the titanium substrate [31] or adding metal or nonmetal ions ( $\text{F}^-$ ,  $\text{Fe}^{3+}$ ,  $\text{Ce}^{3+}$ ,  $\text{CO}^{2+}$ ) [32-35] in the  $\text{PbO}_2$  films.

In this work, we integrated graphene oxide (GO) to decrease the inner stress of the  $\text{PbO}_2$  electrode. Graphene oxide (GO) is a non-traditional soft material with a very high tensile strength and mechanical strength [36], which has been widely applied in polymer and inorganic composite materials [37]. It has the characteristic likeness of polymers, colloids and thin films, and as an amphiphilic molecular structure that can remarkably reduce the interfacial energy. Moreover, it has specific surface area and abundant surface functional groups [38], which makes it easy to disperse in solvents and coordinate to metal oxide. In this study, graphene oxide was doped into the interlayer ( $\text{Sb-SnO}_2$ ) of  $\text{Ti/Sb-SnO}_2\text{-GO/PbO}_2$  electrode as a buffer component to reduce the distortion of the electrode, and increase the affinity between the substrate and the surface layer.

## 2. EXPERIMENTAL

### 2.1 Reagents

All chemicals were reagent grade.  $\text{Pb}(\text{NO}_3)_2$ ,  $\text{N}_2\text{H}_4\cdot\text{H}_2\text{O}$ ,  $\text{HNO}_3$ ,  $\text{SnCl}_4\cdot 5\text{H}_2\text{O}$ ,  $\text{SbCl}_3$  and other reagents were obtained from Sinopharm Chemical Reagent Co. Ltd, China. All reagents were used without further purification and all solutions were prepared with de-ionized (DI) water.

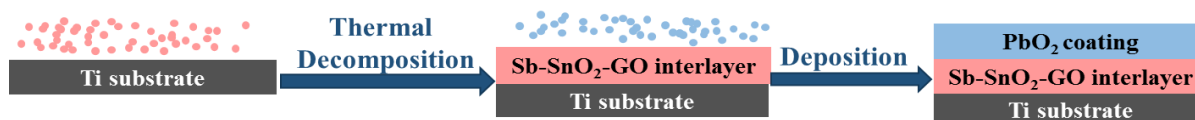
### 2.2 Preparation of $\text{Ti/Sb-SnO}_2\text{-GO/PbO}_2$ electrode

The graphite oxide was prepared by improved Hummers method [39]. 1g graphene oxide was added into 200 mL deionized water and ultrasonically dispersed for 3h to obtain a homogeneous GO aqueous solution (5 mg/mL). High-purity (99.7%) titanium plates (10 mm×60 mm×0.5 mm) were used

as the substrate materials. The titanium sheets were pre-treated by mechanically polishing, ultrasonic cleaning, degreasing with 5% NaOH solution, soaking in 10% H<sub>2</sub>SO<sub>4</sub> for 1 h, and then etching in 10% oxalic acid for 2 h. Finally, it was washed with DI water and kept in 1% oxalic acid solution.

After pretreatment, a Sb-SnO<sub>2</sub>-GO interlayer was fabricated on the titanium substrate by repeated coating and pyrolysis that can be described as following. A mixture of hydrochloric acid (10 mL) and n-butyl alcohol (30 mL) containing SnCl<sub>4</sub>·5H<sub>2</sub>O, SbCl<sub>3</sub> and 1 mL of as-prepared graphene oxide solutions was configured. The pretreated Ti substrate was dipped in the solution using a dip coater, and dried at 130 °C for 10 min, at last calcinated for 15 min in a muffle furnace at 450 °C. This procedure was repeated for the specified times. This gave the Ti/Sb-SnO<sub>2</sub>-GO that was directly used for electrodeposition of PbO<sub>2</sub>.

Electrodeposition of β-PbO<sub>2</sub> was carried out in a single electrochemical cell that was filled with 0.15 M HNO<sub>3</sub> + 0.5 M Pb(NO<sub>3</sub>)<sub>2</sub> + 0.04 M NaF and by the constant current method. Ti/Sb-SnO<sub>2</sub>-GO substrate with an effective working area of 10 mm×10 mm was used as the anode, while the counter electrode was a graphite plate with a geometric size of 20 mm×10 mm. The electrode gap was 15 mm, and magnetic stirring was used to enhance the electrolyte diffusion. The preparation of electrode was optimized by varying deposition current densities, deposition times and deposition temperatures, which were specified in each discussion section. Scheme 1 shows the preparation of Ti/Sb-SnO<sub>2</sub>-GO/PbO<sub>2</sub> electrode.



**Scheme 1** Schematic illustration for the preparation of Ti/Sb-SnO<sub>2</sub>-GO/PbO<sub>2</sub> electrode.

### 2.3 Morphological and electrochemical characterization

The morphology was studied by a scanning electron microscope (SEM, Carl Zeiss AG Ultra Plus). X-ray diffraction data was characterized by a PAN analytical X'Pert Pro X-ray diffractometer with Cu K $\alpha$  ( $\lambda=0.15418$  nm). All the electrochemical behavior of the electrodes is tested on a CS150 electrochemical workstation (Corrtest, Wuhan). In this work, a three-electrode system was used. The as-prepared electrode was used as the working electrode with a test area of 10 mm×10 mm, while the platinum electrode worked as the counter electrode, and the saturated calomel electrode (SCE) worked as the reference electrode. Electrochemical degradation experiments of N<sub>2</sub>H<sub>4</sub>·H<sub>2</sub>O were carried out using a solution of 100 mL of 4.74 mg/L hydrazine hydrate solution. The potential was referred to the reference electrode. The residual concentration of hydrazine was determined according to the reported method [40, 41]. The removal efficiency was calculated as following:

$$\text{Removal efficiency} = \frac{A_0 - A_t}{A_0} \times 100\%$$

$A_0$  is the initial sample's absorbance at 458 nm of the hydrazine that was colorized by p-dimethylaminobenzaldehyde.  $A_t$  is the absorbance of the sample at a given time.

### 3. RESULTS AND DISCUSSION

We investigated the Influence of preparation processes on structure and properties of the electrode, including the coating numbers of Sb-SnO<sub>2</sub>-GO, and the electrodeposition conditions of working layer PbO<sub>2</sub>.

#### 3.1 The coating numbers of interlayer Sb-SnO<sub>2</sub>-GO

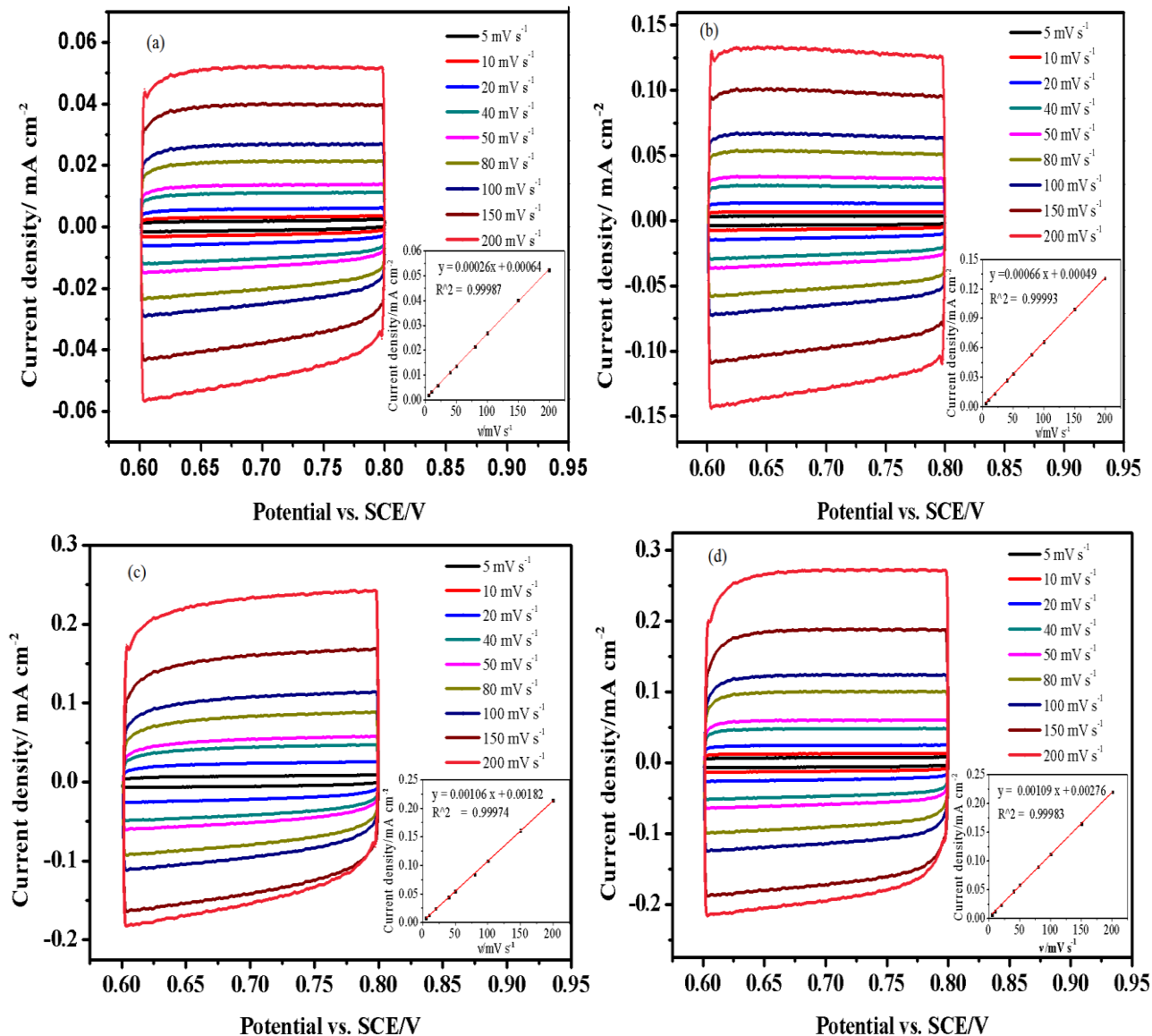


**Figure 1.** Cyclic voltammograms for Ti/Sb-SnO<sub>2</sub>-GO of different coating layers with sweep rates from 5 to 200 mV s<sup>-1</sup> in 0.25 M Na<sub>2</sub>SO<sub>4</sub> solution: (a) 5 layers; (b) 10 layers; (c) 15 layers; (d) 20 layers.

The effect of coating numbers on the substrate was estimated by the relative roughness factor, which was deduced from measuring the cyclic voltammetry (CV) of Ti/Sb-SnO<sub>2</sub>-GO electrodes. Fig.1 illustrates the cyclic voltammograms of electrodes with different coating times in 0.25 M Na<sub>2</sub>SO<sub>4</sub> at the sweep frequency from 5mV/s to 200mV/s within 0.6-0.8V. Because the surface of the electrode is

conductive oxides, the double layer charging current is linearly related to the sweep rate. The insets are plots of the current densities at 0.7 V versus the sweep rates. The actual capacitances of the electrodes are calculated from the slope. Comparing the capacitances with that of a smooth oxide surface ( $60 \mu\text{F}\cdot\text{cm}^{-2}$ ) gives the roughness factor [42], which reflects the real surface area of the electrode.

The roughness factors of the various layers of the electrodes are shown in Fig. 2. As the number of layers increases, the relative roughness factor increases. The value of a substrate coated with 15 layers of metal oxide was 17.6, while the 5-layered one was only 4.3. However, the roughness factor of an electrode coated with 20 layers was not significantly higher than the 15-layered one. Thus, increasing coating times can enhance the roughness and the actual surface area of the metal oxide [43], which enhances the binding strength between the oxides active layer and the interlayer.

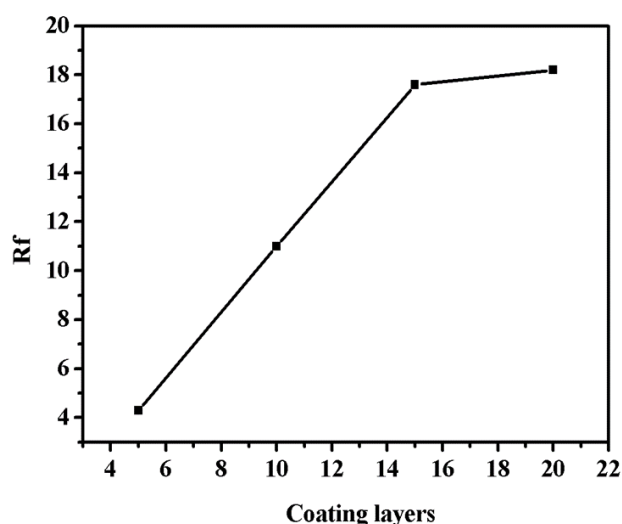


**Figure 2.** The relative roughness factors of Ti/Sb-SnO<sub>2</sub>-GO with different coating layers.

### 3.2 Effect of Electrodeposition Conditions on Electrode Performance

#### 3.2.1 Effect of deposition current density

The PbO<sub>2</sub> films were deposited on the optimized Ti/Sb-SnO<sub>2</sub>-GO substrate under various deposition current densities at 50 °C for 60 minutes. The microstructure of the PbO<sub>2</sub> coatings were observed by SEM. Fig.3 shows the surface morphology of the PbO<sub>2</sub> coatings deposited at different current densities. The PbO<sub>2</sub> coating obtained at 5 mA/cm<sup>2</sup> demonstrate a close pyramid shape, and the interface between the crystallites is regular and clear. With the increasing of the current density, the shape of the crystallite gradually changes from the original Pyramid-like structure to a mixture of Pyramid-like and spherical structure, and the size of the crystals become smaller.

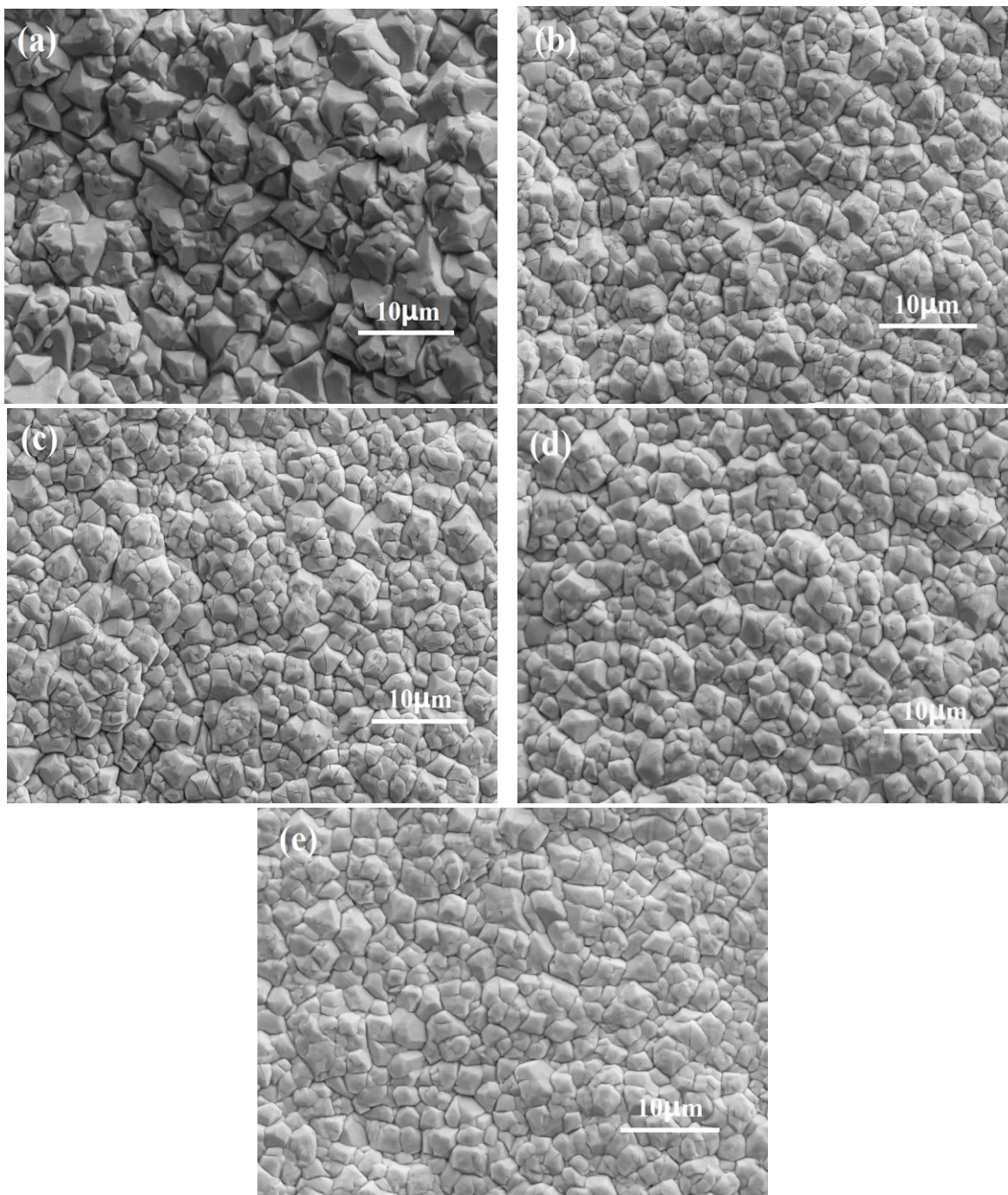


**Figure 3.** SEM of  $\text{PbO}_2$  coatings at various deposition current densities: (a)  $5 \text{ mA/cm}^2$ ; (b)  $10 \text{ mA/cm}^2$ ; (c)  $15 \text{ mA/cm}^2$ ; (d)  $20 \text{ mA/cm}^2$ ; (e)  $25 \text{ mA/cm}^2$ .

In order to further investigate the influence of deposition current density, the depolarization of methylene blue (MB) solution was carried out in a three-electrode cell system, in which 250 mL of MB solution ( $50 \text{ mg} \cdot \text{L}^{-1}$ ) was electro-oxidized under the current density of  $20 \text{ mA/cm}^2$ . The removal ratio of MB at different time is shown in Fig.4. The degradation on the  $5 \text{ mA/cm}^2$  deposited electrode reached 70% within 120 minutes, while other electrodes gave lower value. All the degradation processes are fitted according to the pseudo-first-order reaction model [44] with good linear

relationship. The kinetics constants of degradation for 5, 10, 15, 20, 25 mA/cm<sup>2</sup> deposited electrode are  $1.05 \times 10^{-2} \text{ min}^{-1}$ ,  $9.85 \times 10^{-3} \text{ min}^{-1}$ ,  $7.19 \times 10^{-3} \text{ min}^{-1}$ ,  $6.78 \times 10^{-3} \text{ min}^{-1}$ ,  $7.71 \times 10^{-3} \text{ min}^{-1}$ , respectively. The results showed that the electrode prepared at 5 mA/cm<sup>2</sup> deposition gave the fastest degradation rate.

Considering the microstructure and CV of the electrode, it can be explained that electrode prepared at 5 mA/cm<sup>2</sup> gave the fastest degradation rate, and the reaction rate is related to the electron conduction velocity of different crystallites. The connectivity between the pyramid-shaped microcrystals is better than spherical structure [45]. We determined that the 5 mA/cm<sup>2</sup> was the optimal deposition current density.

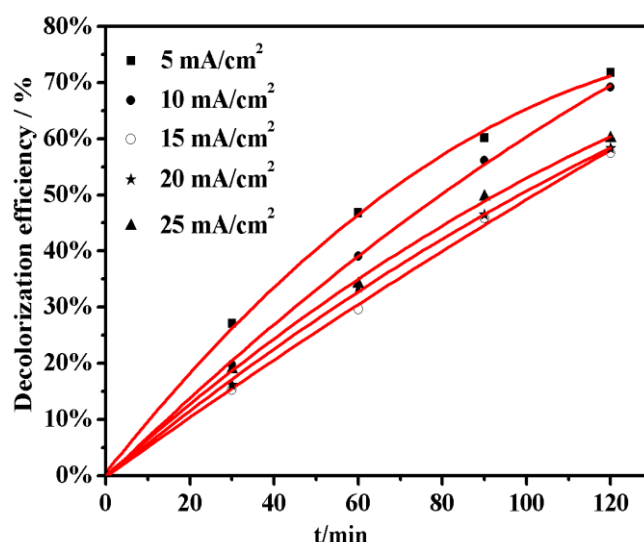
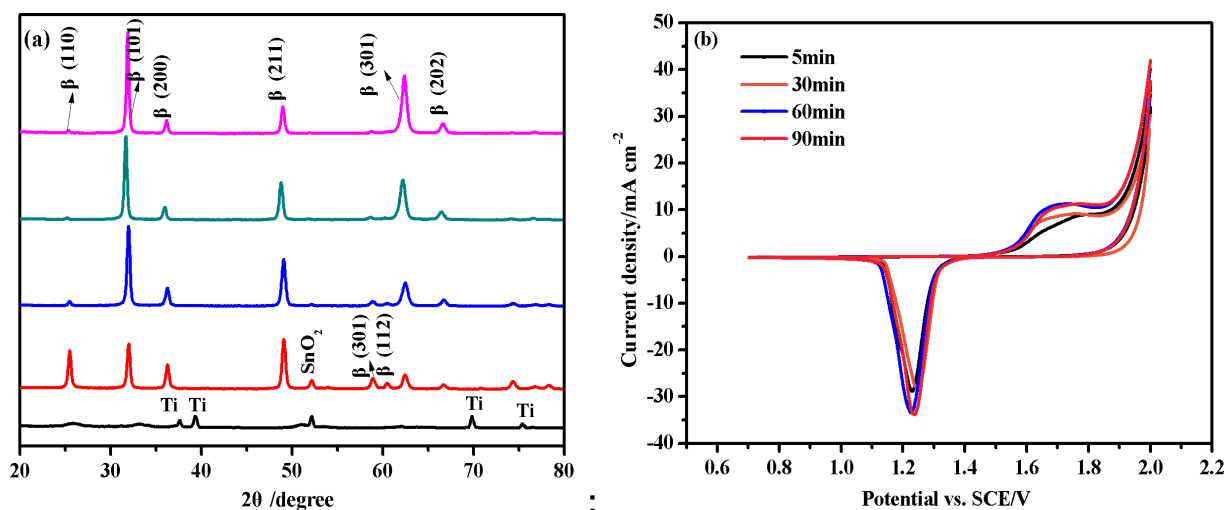


**Figure 4.** Decolorization efficiencies of MB on Ti/Sb–SnO<sub>2</sub>/PbO<sub>2</sub> electrodes deposited at different current densities.

### 3.2.2 Effect of deposition time

X-ray diffractions were employed to determine the crystal characteristics of the PbO<sub>2</sub> coatings. Fig. 5(a) presents the XRD patterns of the PbO<sub>2</sub> electrodes with various deposition time of 5, 30, 60 and 90 min at the optimized current density that was 5 mA/cm<sup>2</sup>. When the deposition time is 5 min, the surface of the substrate is covered with the lead dioxide coating, but there is still a tiny diffraction peak of SnO<sub>2</sub>. It indicates that the coating of tin-antimony oxide is not completely covered. We can assign the diffraction peaks of (110) (200) (211) (301) (202) planes of the β-PbO<sub>2</sub>, and the deposited crystals don't show preferential orientation. The diffraction peak of undercoat SnO<sub>2</sub> disappears when the deposition time is more than 30min. The peaks corresponding to (110), (310), (112) and (321) planes become weaker, while the peak of (101) and (301) planes grow continuously after 30 minutes coating. At the early stage of deposition, lead dioxide crystals grow randomly along the nucleuses that generate on the tin-antimony oxide to form a coating film. When the substrate is completely covered, the film grows along some certain orientations that favorite the crystal growth. The type or intensity of the diffraction peaks does not change obviously after depositing for more than 60 minutes.

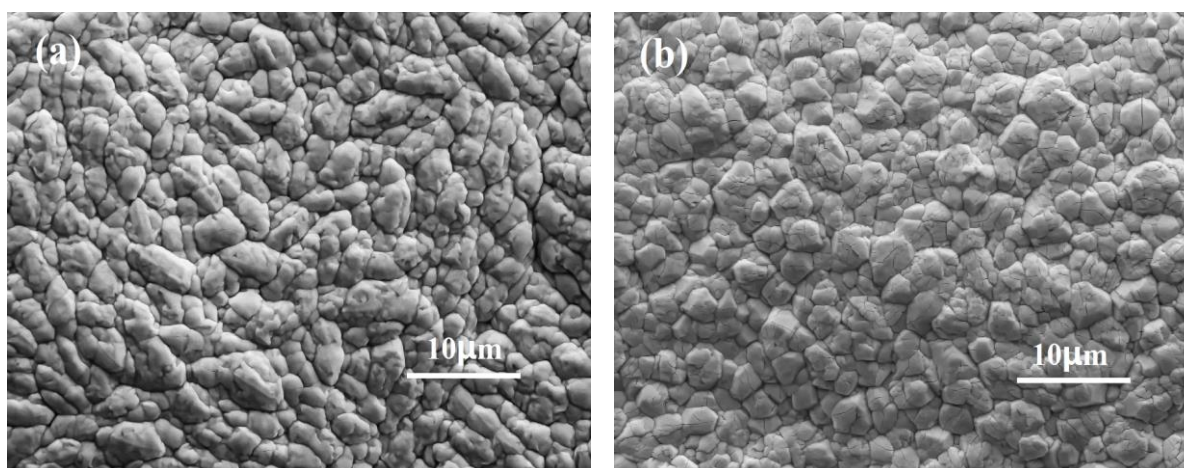
Cyclic voltammograms of the electrodes with different deposition time are shown in Fig.5(b). The oxidation peak current density increases as the deposition time extends, but no improvement can be obtained when the deposition time is longer than 60 minutes. The best deposition time is 60min.



**Figure 5.** (a) XRD diffractograms (b) Cyclic voltammograms of the PbO<sub>2</sub> coatings for different deposition time: (a) 5 min; (b) 30 min; (c) 60 min; (d) 90 min.

### 3.2.3 Effect of deposition temperature

Fig. 6 shows the SEM micrographs of the  $\beta$ -PbO<sub>2</sub> coatings at different deposition temperatures (i.e. 35 °C, 45 °C, 55 °C, 65 °C and 75 °C). The electrodes were prepared at a deposition current density 5 mA/cm<sup>2</sup> for 60 min. The results show that the temperature affects the nucleation and growth of  $\beta$ -PbO<sub>2</sub> crystals. It can be deduced that the preferred orientations of the crystal growth are different at various temperatures, as a result the crystals show different morphology. When the deposition temperature is 35 °C, the crystals on the electrode surface show a worm-like structure. As the temperature raises, the crystallites of  $\beta$ -PbO<sub>2</sub> coating begin to change to an angular pyramid shape. This explanation is supported by our results and others [46, 47]. When the temperature reaches 65 °C, the crystal of the electrode surface shows a compact pyramidal structure and presents a clear interface, which is highly conductive.



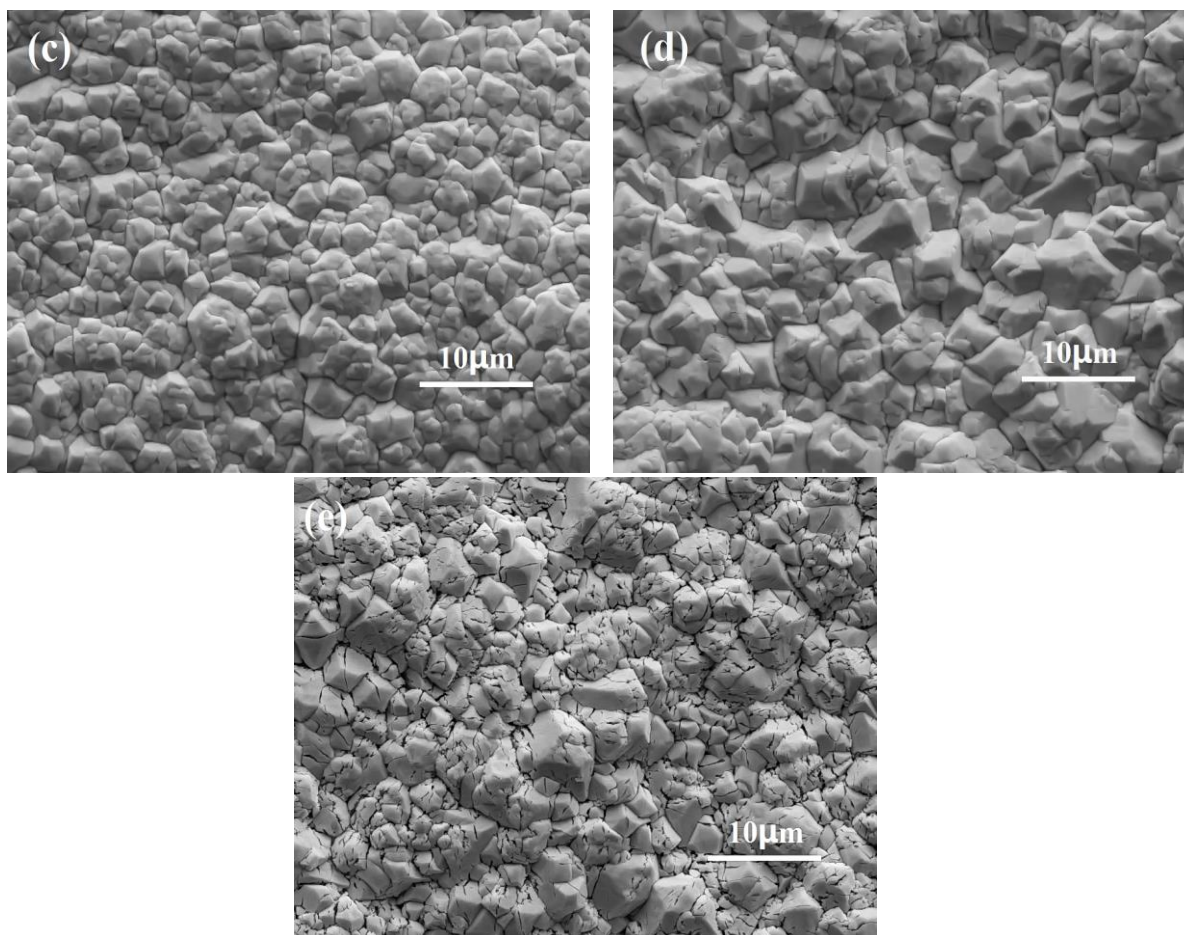


**Figure 6.** SEM of PbO<sub>2</sub> coatings deposited at various temperature: (a) 35 °C; (b) 45 °C; (c) 55 °C; (d) 65 °C; (e) 75 °C.

Moreover, the size of  $\beta$ -PbO<sub>2</sub> crystallites is larger under the higher electrodeposition temperature. However, the surface appears obvious fragmentation and holes at a deposition temperature of 75 °C. This may cause the infiltration of the electrolyte then decline the life of the working electrodes. So the 65 °C is chosen as the optimized deposition temperature.

As shown in Fig.7, the degradation of MB was carried out to further evaluate the effect of electrolyte temperature on the electrocatalytic performance of the electrode. The degradation processes are fitted as the pseudo-first-order reaction model with excellent linear relationship. The kinetics constants of degradation for the 35, 45, 55, 65, 75 °C prepared electrodes are  $7.99 \times 10^{-3} \text{ min}^{-1}$ ,  $9.18 \times 10^{-3} \text{ min}^{-1}$ ,  $1.01 \times 10^{-2} \text{ min}^{-1}$ ,  $1.18 \times 10^{-2} \text{ min}^{-1}$  and  $1.31 \times 10^{-2} \text{ min}^{-1}$ , respectively. This makes sure that the catalytic performance of the electrode benefits from the rising of deposition temperature. Thus, the optimized deposition temperature was determined to be 65 °C.

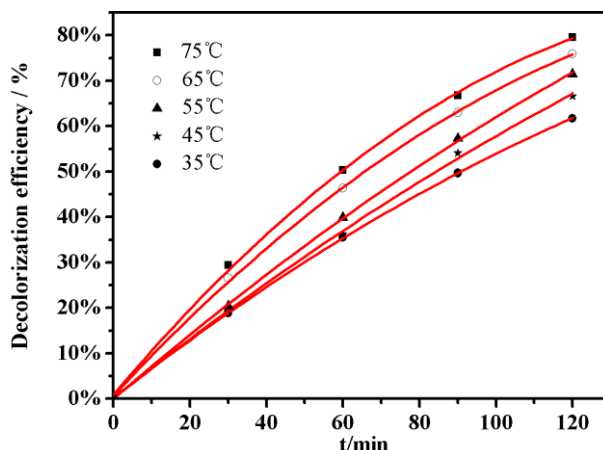


**Figure 7.** Electrochemical decolorization efficiencies of MB using Ti/Sb-SnO<sub>2</sub>-GO/PbO<sub>2</sub> electrodes prepared at different deposition temperatures.

### 3.3 Electrochemical degradation of N<sub>2</sub>H<sub>4</sub>·H<sub>2</sub>O in wastewater over Ti/Sb-SnO<sub>2</sub>-GO/PbO<sub>2</sub> electrode

#### 3.3.1 Optimization of degradation potential

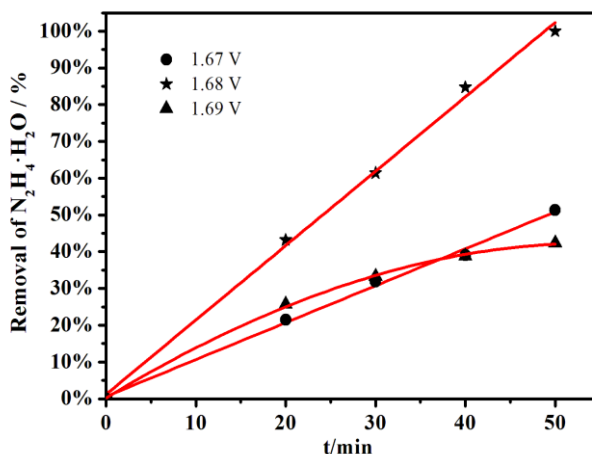


**Figure 8.** The effect of electric potential on N<sub>2</sub>H<sub>4</sub>·H<sub>2</sub>O removal percentage (electrolyte concentration 0.1 mol/L, initial concentration of N<sub>2</sub>H<sub>4</sub>·H<sub>2</sub>O 4.74 mg/L, pH =7, electrode gap 3 mm, room temperature)

To prevent the chemical reduction of lead dioxide electrode, the electro oxidation potential was set at not lower than the oxidation potential of Pb<sup>2+</sup> that is 1.67V. The optimization of reaction potential range for the hydrazine hydrate degradation was 1.67-1.69V. Fig.8 shows that after electrolyzed for 50 minutes, the degradation rates of hydrazine hydrate are 62.6%, 100% and 48.9% at the potentials of 1.67 V, 1.68 V and 1.69 V, respectively. The results indicate that the electrochemical oxidation of hydrazine at 1.67 V and 1.68 V fit to the pseudo-zero-order reaction. The kinetic constants are shown in Table 2 with good linear relationship. At potentials of 1.67 V or 1.68 V, the degradation rates of hydrazine hydrate don't decline with the decreasing of the hydrazine concentration. However, when the electrolysis is performed at 1.69V, the degradation slows down as the reaction proceeds. The

possible reason is that 1.69 V reaches the splitting voltage of water on the  $\beta$ -PbO<sub>2</sub> electrode [48], and the side reaction raises with the concentration of hydrazine hydrate gradually decreases. In summary, 1.68 V is the optimal potential for the removal of N<sub>2</sub>H<sub>4</sub>·H<sub>2</sub>O on the PbO<sub>2</sub> electrode.

**Table 2.** Degradation kinetics constant ( $k/\text{mmol}\cdot\text{dm}^{-3}\cdot\text{min}^{-1}$ ) of N<sub>2</sub>H<sub>4</sub>·H<sub>2</sub>O in different electric potentials.

Potential	1.67V	1.68V	1.69V
$k/\text{mmol}\cdot\text{dm}^{-3}\cdot\text{min}^{-1}$	$9.6\times 10^{-4}$	$1.91\times 10^{-3}$	\
R <sup>2</sup>	0.996	0.996	\

### 3.3.2 Effect of electrode distance

The distance between the anode and the cathode is an important factor in electrolysis. An appropriate electrode gap is helpful to achieve better removal of hydrazine hydrate as well as lower energy consumption. The electrode was tested at the distance of 3 mm, 1cm and 1.5 cm, and the results are shown in Fig.9. Within 50 min, the degradation rate of hydrazine hydrate reaches almost 100% on the electrodes with 3 mm distance. All the degradation processes are fitted according to the pseudo-zero-order reaction model and as listed in Table 3, the kinetics constants on different electrode spacing are  $1.91\times 10^{-3}$ ,  $1.1\times 10^{-3}$  and  $0.9\times 10^{-3}$   $\text{mmol}\cdot\text{dm}^{-3}\cdot\text{min}^{-1}$ . The results show that the electrode spacing significantly affect the removal of hydrazine hydrate, and the efficiency decreases with the increasing of the distance between electrodes. This is because that small gap generates low resistance between the electrodes, and the electric field strength and the current are greater, the removal rates will be enhanced. However, shortening the electrode spacing will increase the real-time flow rate between the electrodes in the industrial application, which may cause a greater erosion of the electrode. Nevertheless, due to the addition of GO in the interlayer Sb-SnO<sub>2</sub>, the PbO<sub>2</sub> electrodes with relatively flexible interlayer can show higher service life.

Interestingly, we find that logarithm of electrode distances ( $\ln \delta$ ) fitted to the kinetics constants ( $k$ ) with the good linear ship (figure 9, b). As the electrolysis cell is a parallel electrode system, this linearship means the reaction rate is related to the electric field strength between the anode and the cathode. The relationship may be valuable to be further investigated.

**Table 3.** Degradation kinetics constant ( $k/\text{mmol}\cdot\text{dm}^{-3}\cdot\text{min}^{-1}$ ) of N<sub>2</sub>H<sub>4</sub>·H<sub>2</sub>O in different electrode gaps.

Electrode gap	3 mm	1 cm	1.5 cm
$k/\text{mmol}\cdot\text{dm}^{-3}\cdot\text{min}^{-1}$	$1.91\times 10^{-3}$	$1.1\times 10^{-3}$	$9\times 10^{-4}$
R <sup>2</sup>	0.997	0.996	0.998

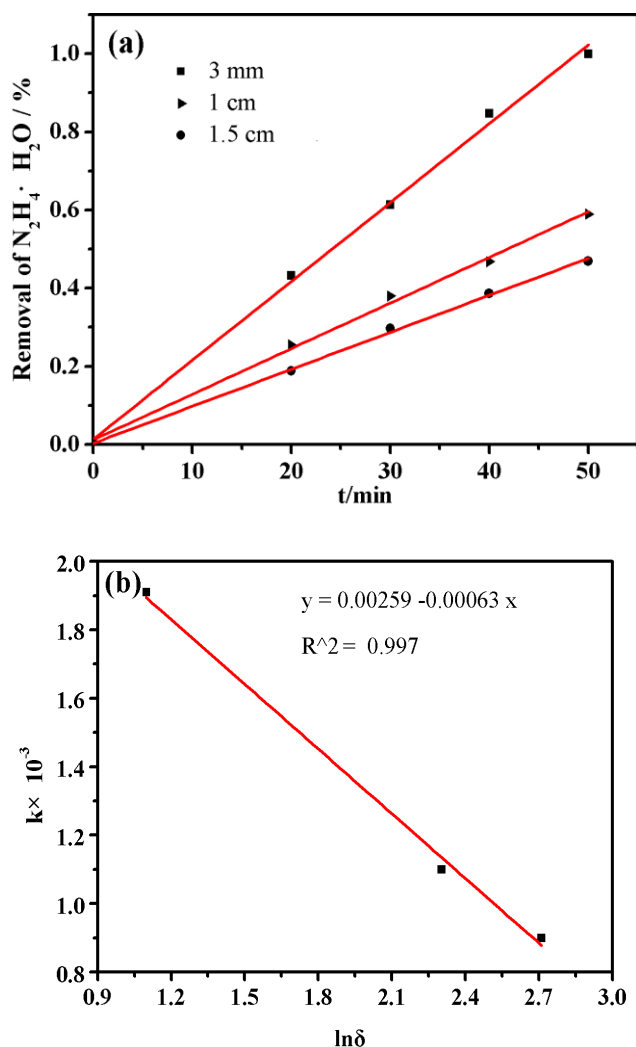


**Figure 9.** (a) The effect of electrode gap on  $N_2H_4 \cdot H_2O$  removal efficiency (b) kinetic constant  $-\ln \delta$ ,  $\delta$  means the electrode gap (electrolyte concentration 0.1 mol/L, initial concentration of  $N_2H_4 \cdot H_2O$  4.74 mg/L, pH = 7, electric potential 1.68 V, room temperature)

#### 4. CONCLUSION

The influence of Ti/Sb-SnO<sub>2</sub>-GO coating times on the electrode performance is investigated. The results show that it is favorable to increase the roughness factor of composite metal oxide layer, which is beneficial to increase the surface area of the electrode and the deposition of the active layer. The important experimental parameters in the deposition process of lead oxide were discussed. The morphologies of electrodes prepared at various current densities are different. The electrodes with pyramid-shaped crystals have higher electrode activity. The crystals of the electrode prepared at 65 °C show a close pyramidal shape, and the electrochemical oxidation performance is the best. Increasing the deposition time in a certain range will increase the coverage of the oxides active layer, and improve electro-catalytic performance of the electrodes.

The effects of potential, electrode spacing and electrolyte concentration on the degradation rate of hydrazine hydrate are discussed. The degradation process at constant potential conforms to zero-

order kinetics. The Ti/Sb-SnO<sub>2</sub>-GO/PbO<sub>2</sub> electrode prepared in this paper has good degradation effect on residual trace hydrazine hydrate in water. The initial concentration of N<sub>2</sub>H<sub>4</sub>·H<sub>2</sub>O 4.74mg/L, in the 1.68V potential, the electrode spacing of 3mm, can be degraded completely within 15min.

## References

1. D. Rajkumar, B. J. Song, J. G. Kim, *Dyes Pigments*, 72 (2007) 1.
2. D. Rajkumar, K. Palanivelu, *J. Hazard. Mater.*, 113 (2004) 123.
3. C.A. Martinez-Huitle, S. Ferro, *Chem. Soc. Rev.*, 35 (2006) 1324.
4. N. Mohan, N. Balasubramanian, C.A. Basha, *J. Hazard. Mater.*, 147 (2007) 644.
5. D. Rajkumar, K. Palanivelu, *Ind. Eng Chem. Res.*, 42 (2003) 1833.
6. J. F. Zhi, H. B. Wang, T. Nakashima, T. N. Rao, A. Fujishima, *J. Phys. Chem. B*, 107 (2003) 13389.
7. A. Maljaei, M. Arami, N.M. Mahmoodi, *Desalination*, 249 (2009) 1074.
8. B. Ntsemdwana, B.B. Mamba, S. Sampath, O.A. Arotiba, *RSC Advances*, 3 (2013) 24473.
9. G. Chen, *Sep. pur. Technol.*, 38 (2004) 11.
10. C. Comninellis, A. Kapalka, S. Malato, S.A. Parsons, L. Poulios, D. Mantzavinos, *J. Chem. Technol. Biot.*, 83 (2008) 769.
11. J. Zhang, D. Li, *Chem. Intermediat.*, 3 (2006) 8.
12. S. Garrod, M.E. Bollard, A.W. Nicholls, S.C. Connor, J. Connelly, J. K. Nicholson, E. Holmes, *Chem. Res. Toxicol.*, 18 (2005) 115.
13. L. Cui, Z.X. Peng, C.F. Ji, J.H. Huang, D.T. Huang, J. Ma, S.P. Zhang, X.H. Qian, Y.F. Xu, *Chem. Commun.*, 50 (2014) 1485.
14. H. Utidjian, H., *J. Occup. med.*, 16 (1974) 107.
15. J.Q. Liu, G.F. Shi, *Environ. Poll. Control.*, 1 (1993) 9.
16. R. Tolba, M. Tian, J. Wen, Z.H. Jiang, A. Chen, *J. Electroanal. Chem.*, 649 (2010) 9.
17. U.T. Un, U. Altay, A.S. Kopalal, U.B. Ogutveren, *Chem. Eng. J.*, 139 (2008) 445.
18. X.Y. Li, Y.H. Cui, Y.J. Feng, Z.M. Xie, J. D. Gu, *Water Res.*, 39 (2005) 1972.
19. L. Zhang, L. Xu, J. He, J. Zhang, *Electrochimica Acta.*, 117 (2014) 192.
20. Y. Duan, Q. Wen, Y. Chen, T. Duan, Y. Zhou, *Appl. Surf. Sci.*, 320 (2014) 746.
21. D. Shao, J. Liang, X.M. Cui, H. Xu, W. Yan, *Chem. Eng. J.*, 244 (2014) 288.
22. B. Correa-Lozano, C. Comninellis, A. De Battisti, *J. Appl. Electrochem.*, 27 (1997), 970.
23. H.B. Zhao, H. Tian, Y.H. Jin, X.J. Cao, *J. Appl. Electrochem.*, 40 (2010) 1307.
24. N.B. Tahar, R. Abdelhedi, A. Savall, *J. Appl. Electrochem.*, 39 (2009) 663.
25. A. Vasebi, M. Partovibakhsh, S.M.T. Bathaee, *J. Power Sources*, 174 (2007) 30.
26. M. Ceraolo, *Ieee T. Power Syst.*, 15 (2000) 1184.
27. M. Zhou, Q. Dai, L. Lei, C. a. Ma and D. Wang, *Environ. Sci. Technol.*, 39 (2005) 363.
28. S.P. Tong, C.A. Ma, H. Feng, *Electrochim. Acta*, 53 (2008) 3002.
29. Y. Zheng, W. Su, S. Chen, X. Wu, X. Chen, *Chem. Eng. J.*, 174 (2011) 304.
30. Y. Chen, H. Li, W. Liu, Y. Tu, Y. Zhang, W. Han, L. Wang, *Chemosphere*, 113 (2014) 48.
31. W. Zhang, H. Kong, H. Lin, H. Lu, W. Huang, J. Yin, Z. Lin, J. Bao, *J. Alloy. Compd.*, 650 (2015) 705.
32. J. Cao, H. Zhao, F. Cao, J. Zhang and C. Cao, *Electrochim. Acta.*, 54 (2009) 2595.
33. L.S. Andrade, L.A.M. Ruotolo, R.C. Rocha-Filho, N. Bocchi, S.R. Biaggio, J. Iniesta, V. García-García, V. Montiel, *Chemosphere*, 66 (2007) 2035.
34. S. Ai, M. Gao, W. Zhang, Q. Wang, Y. Xie, L. Jin, *Talanta*, 2004, 62, 445.
35. A.B. Velichenko, R. Amadelli, E.A. Baranova, D.V. Girenko, F.I. Danilov, *J. Electroanal. Chem.*, 527 (2002) 56.
36. J. Kim, L.J. Cote, F. Kim, W. Yuan, K.R. Shull, J.X. Huang, *J. Am. Chem. Soc.*, 132 (2010) 8180.

37. D.R. Dreyer, S. Park, C.W. Bielawski, R.S. Ruoff, *Chem. Soc. Rev.*, 39 (2010) 228.
38. C.M. Chen, Q.H. Yang, Y.G. Yang, W. Lv, Y.F. Wen, P.X. Hou, M.Z. Wang, H.M. Cheng, *Adv. Mater.*, 21 (2009) 3541.
39. W.S. Hummers Jr, R.E. Offeman, *J. Am. Chem. Soc.*, 80 (1958) 1339.
40. G.W. Watt, J.D. Chrisp, *Anal. Chem.*, 24(1952) 2006.
41. J.S. Zhu, P. Gao, *China Pet. Process. Pe.*, 6 (2015) 110.
42. T. Duan, Y. Chen, Q. Wen, Y. Duan, *RSC Adv.*, 4 (2014) 57463.
43. D. Santos, M.J. Pacheco, A. Gomes, A. Lopes, L. Ciri'aco, *J. App. Electrochem.*, 43 (2013) 407.
44. L. Chang, Y. Zhou, X. Duan, W. Liu, D. Xu, *J. Taiwan Insti. Chem. E.*, 45 (2014) 1338.
45. H. Bi, C. Yu, W. Gao, P. Cao, *Electrochim. Acta*, 113 (2013) 446.
46. X. Li, D. Pletcher, F.C. Walsh, *Electrochim. Acta*, 54 (2009) 4688.
47. O. Shmychkova, T. Luk'yanenko, A. Velichenko, L. Meda, R. Amadelli, *Electrochim. Acta*, 111 (2013) 332.
48. Y. Shen, F. Li, S. Li, D. Liu, L. Fan, Y. Zhang, *Int. J. Electrochem. Sci.*, 7 (2012) 8702.

© 2017 The Authors. Published by ESG ([www.electrochemsci.org](http://www.electrochemsci.org)). This article is an open access article distributed under the terms and conditions of the Creative Commons Attribution license (<http://creativecommons.org/licenses/by/4.0/>).